Radiation Physics and Chemistry 204 (2023) 110708

Contents lists available at ScienceDirect

Radiation Physics and Chemistry

journal homepage: www.elsevier.com/locate/radphyschem

Commissioning of a synchrotron-based proton beam therapy system for use with a Monte Carlo treatment planning system

Juan-Diego Azcona [a,*], Borja Aguilar [a], Álvaro Perales [a], Ramón Polo [a], Daniel Zucca [a], Leticia Irazola [a], Alberto Viñals [a], Pablo Cabello [a], José-Miguel Delgado [a], Diego Pedrero [a], Rocío Bermúdez [a], Roser Fayos-Solá [a], Carlos Huesa-Berral [b], Javier Burguete [b]

[a] Department of Radiation Physics and Radiation Protection, Clínica Universidad de Navarra, Avda, Marquesado de Santa Marta, 1, 28027, Madrid, Spain
[b] Department of Physics and Applied Mathematics, Calle Irunlarrea, 31080, Pamplona, Spain

ARTICLE INFO

Keywords:
Proton therapy
Pencil beam scanning
Commissioning
Beam modelling
Synchrotron
Monte Carlo dose calculation

ABSTRACT

This work tackles the commissioning and validation of a novel combination of a synchrotron-based proton beam therapy system (Hitachi, Ltd.) for use with a Monte Carlo treatment planning system (TPS). Four crucial aspects in this configuration have been investigated: (1) Monte Carlo-based correction performed by the TPS to the measured integrated depth-dose curves (IDD), (2) circular spot modelling with a single Gaussian function to characterize the synchrotron physical spot, which is elliptical, (3) the modelling of the range shifter that enables using only one set of measurements in open beams, and (4) the Monte Carlo dose calculation model in small fields.

Integrated depth-dose curves were measured with a PTW Bragg peak chamber and corrected, with a Monte Carlo model, to account for energy absorbed outside the detector. The elliptical spot was measured by IBA Lynx scintillator, EBT3 films and PTW microDiamond. The accuracy of the TPS (RayStation, RaySearch Laboratories) at spot modelling with a circular Gaussian function was assessed.

The beam model was validated using spread-out Bragg peak (SOBP) fields. We took single-point doses at several depths through the central axis using a PTW Farmer chamber, for fields between 2 × 2cm and 30 × 30cm. We checked the range-shifter modelling from open-beam data. We tested clinical cases with film and an ionization chamber array (IBA Matrix).

Sigma differences for spots fitted using 2D images and 1D profiles to elliptical and circular Gaussian models were below 0.22 mm. Differences between SOBP measurements at single points and TPS calculations for all fields between 5 × 5 and 30 × 30cm were below 2.3%. Smaller fields had larger differences: up to 3.8% in the 2 × 2cm field. Mean differences at several depths along the central axis were generally below 1%. Differences in range-shifter doses were below 2.4%. Gamma test (3%, 3 mm) results for clinical cases were generally above 95% for Matrix and film.

Approaches for modelling synchrotron proton beams have been validated. Dose values for open and range-shifter fields demonstrate accurate Monte Carlo correction for IDDs. Elliptical spots can be successfully modelled using a circular Gaussian, which is accurate for patient calculations and can be used for small fields. A double-Gaussian spot can improve small-field calculations. The range-shifter modelling approach, which reduces clinical commissioning time, is adequate.

1. Introduction

Proton therapy delivered with pencil beam scanning is nowadays becoming more sought-after in hospitals because it better enables conformation of the absorbed dose to the tumour, introducing the possibility of intensity modulated proton therapy (IMPT) (Farr et al., 2021; Moyers et al., 2020; Arjomandy et al., 2019). In addition to modulating the fluence of the beam, as done in intensity modulated radiation therapy (IMRT) and volumetric modulated arc therapy (VMAT), IMPT provides additional modulation of the dose with the

* Corresponding author.
E-mail address: jazcona@unav.es (J.-D. Azcona).

https://doi.org/10.1016/j.radphyschem.2022.110708
Received 1 May 2022; Received in revised form 28 November 2022; Accepted 5 December 2022
Available online 6 December 2022

penetration depth of the beam, which is achieved by controlling the energy of the proton beam. Cyclotrons and synchrotrons are the two types of accelerators that provide proton beams useful for therapy. Cyclotrons are fixed-energy machines. The beam exiting the cyclotron must be filtered in the energy selection system to reduce the energy to the level required for the depth of treatment. With synchrotrons the user can control the beam energy, and no energy degradation system is required. Therefore, a synchrotron produces proton beams with narrower Bragg peaks, in the proximal-to-distal distance, than does a cyclotron, and spot sizes are potentially smaller.

A synchrotron-based proton therapy system (Hitachi, Ltd., Japan) that uses pencil beam scanning (PBS) as delivery technique has recently been installed in the *Clínica Universidad de Navarra* hospital in Madrid (Spain). Pencil beam scanning delivery consists of a narrow proton beam that irradiates the patient. Just before exiting the nozzle, the pencil beam is laterally deflected in two orthogonal directions by two scanning magnets. For proton beam facilities, the set of data required for clinical commissioning and beam modelling usually comprises: (1) integrated depth dose (IDD) curves, (2) spot profiles (crossplane and inplane), (3) absolute dose values and, (4) geometric data on the nozzle, including the virtual source-to-axis distance (VSAD). There are several published works that describe the methods and detectors required for commissioning a proton beam facility (Grevillot et al., 2018; Farr et al., 2018; Lin et al., 2013; Gillin et al., 2010; Dong, 2015; Saini et al., 2016).

Integrated depth dose (IDD) curves provide a relative measurement of the dose per area product. The IDD curves are measured by integrating the charge released by the primary beam at a given depth. The Bragg peak chamber is the detector of choice for measuring this quantity, which is a large diameter (typically between 8 and 12 cm) plane parallel ionization chamber. The dose per area product provides a measurement in a proton pencil beam which is equivalent to a percent depth dose in an extended field, by means of the reciprocity principle (ICRU International Commission on Radiation Units and Measurements, 1984). Because the chamber volume is finite, and the beam interacts through nuclear reactions and high angle nuclear scattering, thus also releasing energy outside the chamber volume, a correction is needed to calculate the true IDD from the measured one (Gottschalk, 2018; Gillin et al., 2010).

The section of a proton pencil beam orthogonal to its axis (spot in air) is often modelled with a Gaussian function, although it can also be modelled with a double Gaussian function (Zhu et al., 2013). The sigma of the Gaussian distribution increases with decreasing energy. This is because proton interactions consequent upon multiple Coulomb scattering events with nuclei are much more likely at lower energies, and, more importantly, the scattering angle increases with the inverse of the energy. The total stopping power increases with decreasing energy. According to the Bethe-Bloch formula (Newhauser and Zhang, 2015), the electronic stopping power in air increases with decreasing proton beam energy: for the same number of incident protons in the same medium, a low energy beam releases more energy than a high energy beam. A similar, although more pronounced trend is observed with the nuclear component of the stopping power.

When working with proton beams, it is necessary to calibrate beam monitors at different energy levels (Palmans, 2018). In this way, the absorbed dose in a reference condition of a mono-energetic beam can be related to the number of monitor units (MU) delivered. Monitor chambers are located in the nozzle. The electric current generated in the chamber is converted to frequency (via a current to frequency converter) and so the accumulated number of pulses directly corresponds to the charge collected in the monitor chamber. A MU is directly proportional to the charge collected in the chamber, irrespective of the energy of the incident proton that produced the ionization. Because of the relationship between the electronic part of the stopping power (typically, for most monitor chambers, we are concerned with the stopping power in air) and the proton energy, the higher the energy of the proton beam, the more protons needed to produce one MU. Therefore, the number of MUs depends on the proton beam energy, and so the Treatment Planning System (TPS) needs the proton energy specific constants of proportionality between MU and number of protons for every individual energy-level that the synchrotron can output at.

The TPS used is RayStation (RaySearch Laboratories AB, Sweden), which uses a Monte Carlo dose calculation algorithm. To our knowledge, this configuration of accelerator and TPS is currently used by only a handful of institutions. Beyond the use of a synchrotron as opposed to a cyclotron, some of the unique characteristics of this configuration are as follows. First, RayStation provides a Monte Carlo correction for a lack of signal from the Bragg peak chamber used to measure the IDD. The amount of correction depends on the chamber diameter. Second, in a synchrotron, spots are slightly elliptical due to beam optics, and the orientation of the ellipse changes with the angle of the gantry. Nevertheless, the spot is modelled with a circular single-Gaussian function using two measured orthogonal profiles. Third, RayStation models a range shifter, which is to be interposed between the beam and the patient, from that range shifter's chemical composition, mass density and ionization potential. This approach makes it unnecessary to create separate beam models for the open beam and for beams used in association with each of various range shifters, with each of these models being based on specific IDDs, spot profiles and absolute dose values.

The aim of this paper is to describe the equipment and methods used for the clinical commissioning of synchrotron-generated proton beams. We will place emphasis on testing the validity of several corrections, approximations, and approaches in the beam modelling process: (1) Monte Carlo based IDD correction, (2) circular spot modelling with a single Gaussian function to characterize the physical spot, which is elliptical, (3) the modelling of the range shifter, and (4) the Monte Carlo model for dose calculation in small fields. With regard to this final point, we will address the potential need for additional refinements to spot modelling for dose calculation in these situations.

Validation measurements to test the model in spread-out Bragg peaks (SOBP) and clinical fields will also be presented. The work of Saini et al. (2017) presented a set of validation measurements for the Monte Carlo algorithm used in a previous version of RayStation. Compared to this paper, our work extends the validation in homogeneous fields to small field sizes. The accuracy of the TPS when modelling different tissue inhomogeneities will be the focus of a separate paper.

2. Material and methods

2.1. Proton therapy system

The proton therapy system installed at our hospital is the Hitachi ProBeat-CR (Hitachi, Ltd., Japan). This consists of a compact synchrotron that produces proton beams with 98 different commissioned energy levels, between 70.2 and 228.7 MeV, corresponding to nominal R_{90} distal ranges of 3.9 and 32.4 cm in water, respectively. Here, R_{90} is defined as the depth in water at which the proton beam delivers 90% of the dose at the Bragg peak. The steps between commissioned energies are smaller at lower energy because of less range straggling at shallower depths, resulting in narrower Bragg peaks in the proximal-to-distal direction. The current configuration of the system includes a compact 360-degree gantry. The system has integrated image guidance systems including cone beam CT, orthogonal x-ray imaging, and fluoroscopy, which, in conjunction with fiducial markers, enable treatment with real-time respiratory-gating for moving tumours. The facility is designed in such a way that at a later date it can be expanded to include a second gantry room, whose beam would be supplied by the same synchrotron. The paper by Gillin et al., (2010) describes several interlocks used by a similar system to ours to ensure the accuracy of the beam energy, spot position and number of monitor units (MU). A quality assurance (QA) program is established comprising daily, weekly, monthly and annual tests. Daily tests include checking energy and spot position and size. Absolute dose values per MU are also checked on a daily basis using an

ionization chamber. Linearity of the monitor chamber outputs was also checked during commissioning and is included in the monthly QA tests.

2.2. Treatment planning system

Beam modelling and patient treatment planning was done in RayStation (RaySearch Laboratories AB, Sweden) version 9B. To build a model, RayStation requires values for only a subset of energies, with a spacing of about 10 MeV, whose IDD, spot profiles and absolute dose values are to be provided. However, we supplied RayStation with values obtained for all 98 available energy levels. This is a different approach to the one followed by Gillin et al., (2010), who generated with Monte Carlo the beam data used for building the model.

RayStation modelling for the spot uses two orthogonal profiles. The spot in our synchrotron-generated proton beam is slightly elliptical, and, according to the Hitachi specifications, the ratio between the sigma values of major and minor axes should be less than 1.1. Although an elliptical spot could be modelled in RayStation, this would not be practical because the ellipse orientation rotates with the gantry, so a circular model would be expected to represent the best compromise for all gantry angles.

The TPS has two dose calculation algorithms: pencil beam and Monte Carlo. We always use the Monte Carlo algorithm for patient-specific optimization and dose calculations because of its superior accuracy (Paganetti, 2012), especially in highly inhomogeneous anatomic areas, such as lung (Taylor et al., 2017). Monte Carlo dose calculation accuracy depends on its actual implementation. In RayStation, the pencil beam algorithm uses the infinite slab approximation, which entails a more severe impact in patients with large lateral inhomogeneities (RayStation Reference Manual). This approximation is not used in RayStation Monte Carlo, whose accuracy is thus expected to be better for patient dose calculations. For this reason, the validation results presented here are based on the Monte Carlo dose calculation algorithm, because this is the algorithm we use in clinical situations.

2.3. Integrated depth-dose curves (IDD)

2.3.1. Equipment

Integrated depth-dose (IDD) curves were measured using a PTW 34070 Bragg peak chamber in combination with a PTW Freiburg, model MP3-PL water tank (PTW Freiburg, Germany).

We checked the homogeneity of the chamber response by directing the same beam spot to different points in the chamber (see Kuess et al., 2017). The linearity of the response of the Bragg peak chamber was checked. Polarity and ion recombination effects of the chamber were also evaluated at different depths and energy levels.

2.3.2. Setup

The setup for IDD measurement is with the gantry at 90°: the beam is horizontal. The scanning system resolution is 0.1 mm. Prior to scanning, we carried out QA controls on the water tank to check that when the detector was moved, the displacements were accurate. We also checked the water tank and chamber alignment to ensure that detector motion was parallel to the proton pencil beam. The global reproducibility of the system was checked by repeating the setup and measurements at 19 different energy levels, which covered the full range of energy levels available from the synchrotron. IDD measurements at these 19 energy levels were subsequently taken again as part of clinical commissioning. We used the constancy of R_{90} values to assess measurement reproducibility.

2.3.3. Measurement

IDD measurements were acquired without any additional equipment interposed between the beam and the Bragg peak chamber. We did not use a reference chamber; instead, we used the PTW Freiburg MP3-PL water tank trigger, which uses a signal obtained from the magnetic sextupole indicating that the synchrotron is ready for beam extraction. We ensured that, for each point in the IDD curve, the chamber integrated the electric charge induced by the beam providing 12 MUs.

2.3.4. Validation of the Monte Carlo correction to the measured IDDs

RayStation provides a Monte Carlo-based correction to the signal collected by the Bragg peak chamber. This correction was validated through the measurements in SOBP fields reported later in this paper. Indeed, any inaccuracy in the determination of the correction would end up in relevant differences when summing up pristine Bragg peak curves resulting in a calculated SOBP field, as compared to measured values.

The data acquired by the Bragg peak chamber are, in fact, depth ionization curves, and a conversion to dose is needed, as recommended in TRS-398. This was done by us before supplying the curves to RayStation. We used the formula in the IAEA TRS-398 document, where the stopping power ratio of water-to-air $s_{w,air}$ is expressed in terms of the residual range R_{res} (distances in cm):

$$s_{w,air} = 1.137 - 4.265 \times 10^{-5} \times R_{res} + \frac{1.84 \times 10^{-3}}{R_{res}} \quad (1)$$

The residual range is defined at each point in the IDD curve, and it is defined as the difference in depths between a certain point and the practical range (TRS-398).

2.4. Spots

2.4.1. Equipment and setup

Spots were measured, for every energy available from the synchrotron, using the IBA Lynx scintillator detector (IBA Dosimetry GmbH, Germany). Measurements were used for beam modelling in RayStation. The Lynx scintillator has an active area of detection of 30 cm × 30 cm with a spatial resolution of 0.5 mm. It was aligned with its axes parallel to the gantry reference system axes, and orthogonal to the beam's incidence. The scintillator was commissioned in terms of linearity, reproducibility of its response, homogeneity, dependence of response on iris aperture, and geometric distortion. Commissioning followed the procedures described in the work of Russo et al. (2017).

We validated Lynx measurements by comparison with measurements with radiochromic film (Gafchromic EBT3, Ashland, Bridgewater, NJ) and with a solid-state detector (the PTW 60019 microDiamond).

2.4.2. Validation of the spot modelling approach

We used the set of measurements obtained with various detectors to assess the approximations taken to model the elliptical spot to a 2D circular Gaussian using two profiles obtained through the gantry axes. A 2D Gaussian is characterized by the two sigma values corresponding to the major and minor axes of an ellipse. We checked the validity of the RayStation's approach by comparing:

- Elliptical 2D Gaussian fits based on the full 2D image (Lynx and EBT3 images) with elliptical 1D fits based on two orthogonal profiles (from Lynx, EBT3 and microDiamond).
- The average sigma of 1D fits with the sigma of a 2D fit to a circular Gaussian. In this way we checked the feasibility of modelling the physical spot with a circular Gaussian distribution defined by two orthogonal profiles each with its own sigma determined by the axes of the gantry.

2.4.3. Validation of Lynx measured spots with EBT3 radiochromic films. Analysis of circular and elliptical fits

For nine energy levels representative of what is available from the synchrotron (71.2, 89.3, 108.4, 126.6, 140.8, 160.9, 178.0, 194.9, and 218.7 MeV), we performed a 1D fit to a Gaussian distribution through the gantry axes. We also performed a 2D fit to a Gaussian distribution using the full 2D image, using both elliptical and circular Gaussian functions. We compared the sigma values obtained with both detectors

in the different fits. In addition, the spot orientation angle relative to the gantry axes was calculated. The spatial resolution used in the film analysis was 75 dpi (0.3387 mm).

2.4.4. Profile validation with respect to microDiamond

We measured crossplane and inplane spot profiles in air at three different energy levels (71.2, 140.8, and 218.7 MeV) with a PTW 60019 microDiamond detector. The detector was aligned such that its axis of revolution was parallel to the scan direction, keeping the direction of movement forward (the top of the detector was facing forward when the detector was in motion). In this orientation the cross-section of the detector is 1 μm, which minimizes the profile smoothing effect. In this way, spot profiles acquired with the microDiamond are considered to be "true" profiles and no deconvolution procedure is required. Spatial resolution was 0.2 mm. As in the previous case in 1D scanning, scan directions follow the gantry axes. We did a 1D fit of both profiles to a Gaussian distribution and compared the sigmas with those from the respective fits from the Lynx and EBT3 films.

2.4.5. Measurement of spot size dependence on gantry angle

Because of beam optics, the properties of the spot depend on the angle of the gantry and so, to assess the model's accuracy it is also necessary to check the spot over a full range of gantry angles. We analysed spot size with respect to 12 different gantry angles: 180, 210, 240, 270, 300, 330, 0, 30, 60, 90, 120 and 150°. We used film to measure the size of the spot in terms of the major and minor sigma values of the ellipse for three different beam energies: 71.2, 140.8 and 218.7 MeV.

2.4.6. Measurements for beam modeling

Spot measurements were acquired using the Lynx scintillator at five different source-to-detector distances (SDD): with the detector at the isocenter, at 10 and 20 cm from the isocenter towards the source, and at 10 and 20 cm from the isocenter away from the source. The detector outputs a 2D image from which beam profiles can be extracted.

2.5. Absolute dose values

2.5.1. Equipment

We measured the absolute dose with a plane-parallel chamber (the Advanced Markus 34045, manufactured by PTW Freiburg) on an extended field. The diameter of the electrodes is 5 mm, and the effective point of measurement is located at the inner side of the entrance electrode.

The chamber was calibrated in terms of $N_{D,w}$ in ^{60}Co at a Secondary Standard Dosimetry Laboratory (SSDL). We measured the k_Q by cross-calibration with a Farmer chamber for a high-energy (228.7 MeV) mono-energetic proton beam, as recommended by Palmans (2018). We evaluated polarity and recombination for 19 beams over a range of energy levels spaced in steps of 10 MeV or less, covering the full range of available energies.

2.5.2. Setup and measurements

The goal was to establish the energy-specific relationship between the MUs delivered by the system and the absorbed dose under the specific setup conditions (in water) required by the TPS. Using the Advanced Markus chamber in the PTW Freiburg MP3-PL water tank, we measured the absolute dose values for mono-energetic beams at all 98 energy levels available from the synchrotron. We used an extended 10 cm × 10 cm field, with the spots spaced 2.5 mm in a square pattern. Measurement points were in the plateau region, which, according to RaySearch recommendations, is at a depth approximately halfway between 1 cm and the depth at which the Bragg peak occurs.

RayStation uses these data to determine, for a given energy level, the number of simulated protons needed to produce one MU in the monitor chamber. These values are used in the Monte Carlo simulation that calculates the dose required for each patient. With this energy level dependent relationship, the TPS calculates the MUs required to treat a patient's tumour with the prescribed dose. This is a different approach to the one followed by Gillin et al., (2010), who used a Bragg peak chamber, previously cross calibrated with a Farmer chamber in passively scattered proton beams, to measure absolute integral dose values in single spots.

2.6. Reference dose values according to TRS-398

We followed the procedure described in TRS-398 (International Atomic Energy Agency IAEA, 2000) to determine the reference dose value. We measured, at a depth of 15 cm, the dose resulting from a 10 cm × 10 cm SOBP field extended in water at depth between 10 and 20 cm. We used a Farmer chamber (model 30013 by PTW Freiburg) calibrated at a SSDL in ^{60}Co in terms of dose to water ($N_{D,w}$), with the k_Q value as tabulated in TRS-398. The TRS-398 k_Q values are for reference conditions, that is, the k_Q correction is determined for SOBP beams. The linearity of the response of the Farmer ionization chamber was checked. Polarity and recombination corrections were established for use with all SOBP fields.

2.7. Range shifter modelling

Several TPSs in the field of proton therapy use separate sets of IDD curves, spot profiles and absolute dose values to build different, independent models for open beams and for each one of the range shifters available in the facility. The RaySearch TPS, however, can model the range shifter from user-provided data on the range shifter's chemical composition, mass density, and ionization potential. Consequently, only the set of measurements corresponding to the open beam is needed for beam commissioning.

From the chemical composition, density, and ionization potential of the constituents of the range shifter, the ionization potential for the range shifter was calculated using the Bragg additivity rule. Our range shifter is 3.9 cm thick and, according to Hitachi documentation, has the chemical composition $(C_{15}\ H_{17}N)_n$ and has a mass density of 1.05 gr/cm^3.

The range shifter was validated by comparing measurements and calculations for absolute dose values measured with the 10 cm × 10 cm x 10 cm dose cube described in TRS-398, with the same setup as for the reference dosimetry test, but with the chamber positioned at 11 cm depth in water and the range shifter inserted.

Several IDD curves were also acquired for nine energy levels (89.3, 108.4, 126.6, 142.5, 160.9, 178.0, 194.9, 211.0 and 228.7 MeV). Spot-in-air profiles were obtained for five energy levels (89.3, 117.7, 144.1, 187.5 and 228.7 MeV).

2.8. Validation measurements

2.8.1. SOBP fields

In order to validate the RayStation model, we made various tests. One of these was to measure absolute dose values in the center of SOBP curves. In another test, we measured the absolute dose at several points along the central axes of several SOBP curves. These tests provide evidence of the goodness of the Monte Carlo correction performed by RayStation to the measured IDDs. In both cases, measurements were acquired using a Farmer chamber in several field sizes and SOBP widths and depths. The Farmer chamber was chosen for these sets of measurements because TRS-398 provides a Monte-Carlo-calculated k_Q factor for SOBP measurements. However, we did not measure all fields with a Farmer chamber; 2 cm × 2 cm and 3 cm × 3 cm fields were measured using a PTW 31021 Semiflex 3D (0.07 cm^3 volume) and a PTW 31016 PinPoint 3D (0.016 cm^3 volume) chamber. The k_Q factors for these two chambers were derived by comparison on a SOBP field with the Farmer measurements.

For the measurements in the center of the SOBP, we used the

following combinations of field sizes and SOBP depths and widths:

- Field sizes were 2, 3, 5, 7, 10, 15, 20 and 30 cm,
- SOBP depths were between 5 and 10, 10 and 20, 15 and 20, and 20 and 30 cm.

Values along the central axis were obtained for the field sizes of side 5, 10 and 20 cm, at the following depths:

- SOBP between 5 and 10 cm: Depths every 1 cm between 3.5 and 10.5 cm,
- SOBP between 10 and 20 cm: Depths every 2 cm between 3 and 21 cm,
- SOBP between 15 and 20 cm: Depths of 3, 6, 9, 11, 14, 16, 17.5, 19 and 21 cm.

Measurements were performed using a Farmer ionization chamber. Polarity and recombination corrections were established for the three chambers employed with SOBP beams.

2.8.2. Spot profiles in water

We also took some measurements of spot profiles in water. We acquired crossplane and inplane profiles for three energy levels (70.2, 140.8 and 228.7 MeV) at the following depths:

- 70.2 MeV: 13, 25 and 38 mm (inplane); 23.3, 31.7 and 37.5 mm (crossplane),
- 142.5 MeV: 47, 93 and 140 mm (crossplane and inplane),
- 228.7 MeV: 108, 216, and 324 mm (inplane); 104, 212 and 324 mm (crossplane).

2.8.3. Validation of point dose calculations in special situations

The accuracy of the dose calculation model was assessed for the special situations of oblique incidence, off axis doses and extended distance doses. The setup for these point dose measurements was:

Off axis dose calculations: Four 5 cm $\times$ 5 cm fields located at the corners of a square, centered at $\pm$ 12.5 cm in crossplane and inplane, with a 10 cm width SOBP ranging from 10 to 20 cm depth in water were measured with a Farmer chamber located at 15 cm depth.

Oblique incidence: A 20 cm $\times$ 5 cm field was modelled with oblique incidence (45°) on the water tank. Three points along the field axis at 14.1, 17.7 and 21.2 cm depth were measured.

Extended distance dose calculation: The field described in TRS-398 for checking the reference dose rate was also used to measure the point dose with the Farmer chamber in three locations: at the isocenter, displaced from the isocenter by 20 cm towards the source, and displaced from the isocenter by 15 cm away from the source. In addition, the test was repeated with the 3.9 cm range shifter inserted. The only setup difference with the range shifter was that the isocenter position of the chamber was at a depth of 11 cm depth in water; for the displacements, the water tank was again shifted 20 cm towards the source and 15 cm away from the source (chamber at a depth of 11 cm in water).

2.8.4. Validation of the model using clinical scenarios

Once we had the beam model available for dose calculation on patient images, we prepared some treatment plans for different localizations and site areas, involving different field sizes and energies. We did a validation of those clinical plans using radiochromic film, and the IBA Matrix 2D array (IBA Dosimetry GmbH, Germany), which is based on ionization chambers. We did these measurements in acrylic.

3. Results

3.1. Integrated depth-dose (IDD) curves

The homogeneity of the response of the Bragg peak chamber is expressed by the ratio of the standard deviation divided by the mean of the charge measurements. This ratio was 0.14% for all the measurements performed within a 1 cm $\times$ 1 cm square centered at the geometrical center of the Bragg peak chamber. The homogeneity of the response of the Bragg peak chamber makes it suitable for IDD measurements. The linearity of the response of the Bragg peak chamber was also analysed by a linear regression whose R^2 was unity.

The assessment of recombination corrections with two sets of pairs of voltages (300 and 150V, and 400 and 200V) showed that under the assumption that the beam is continuous there was a difference of 0.3% in the calculated values using both sets of pairs of values, whereas under the assumption that the beam is pulsed this difference among both calculations was 0.8%. Therefore, we confirmed that the beam can be considered to be continuous for the purposes of dosimetry, a finding that is in line with the TRS-398 recommendations for synchrotron beams.

In all evaluated cases - a wide range of energy levels and depths - the recombination corrections of the Bragg peak chamber were within 1.000 and 1.002. The polarity corrections for the same energies and depths were within 0.999 and 1.002. Because the polarity and recombination effects are so small, measured IDD curves were not corrected for these effects in the beam model.

The measured IDD curves were used to determine distal R_{90} values. System reproducibility was assessed using these ranges to be within $\pm$0.1 mm in all cases. These R_{90} values were compared to the nominal ranges provided by Hitachi. Differences found were always within the limits of -0.9 and $+$ 2.0 mm. More importantly, the differences in the range shift between adjacent energy levels (measured range shift versus intended range shift) were always within 0.3 mm. This difference was in general smaller at lower energies. Fig. 1 illustrates how a measured IDD for a 228.7 MeV pencil beam compares with the Monte Carlo corrected curve in our installation. The differences between the curves reach 5% at 200 mm depth.

3.2. Spots

3.2.1. Validation of Lynx-measured spots with EBT3 films and microDiamond. Analysis of circular and elliptical fits

This section discusses the measurement of spots in air for beam characterization. We calculated the sigmas for elliptical Gaussian 1D and 2D fits. The sigmas of the 2D fit correspond to the major and minor axes of the ellipse; the sigmas for the 1D fit correspond to the axes of the detector, which are aligned with the gantry axes. The agreement in the

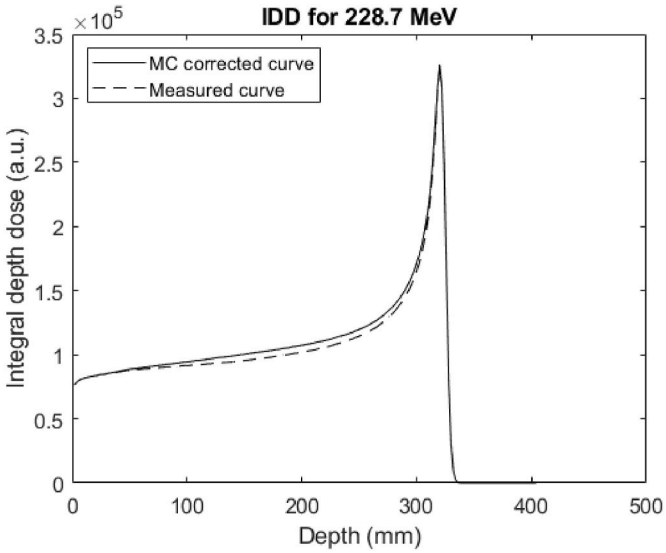

Fig. 1. Measured IDD for 228.7 MeV compared with the Monte Carlo corrected curve.

pairs of sigmas (from 1D and 2D fitting) between the Lynx and the EBT3 films showed differences that were generally less than 0.2 mm and always less than 0.3 mm. Ellipticity, calculated as the ratio of the sigmas (major divided by minor), was always below 1.1 both for Lynx and the EBT3 measurements. The ellipticity of the spot was observed to increase with energy. Differences in the major and minor sigmas between the 1D fit and the 2D fit were generally less than 0.2 mm and always less than 0.3 mm, both for the Lynx and the EBT3 data. Table 1 shows these data for three of the nine energy levels analysed.

Table 2 presents the data for the sigmas and their mean from a 1D fit as well as the sigma for a 2D circular Gaussian fit, for the nine energy levels studied. For a given energy scenario, the values of sigma as determined by the three detectors are always within 0.2 mm of each other. Differences between the average of the two sigmas calculated with the 1D fit and the single sigma of the 2D circular Gaussian fit are never more than 0.2 mm.

3.2.2. Spot size dependence on gantry angle

With respect to how spot size varies with gantry angle, we found that, for the three energies evaluated, the sigma variation with a single Gaussian fit was always less than 0.21 mm, as shown in Table 3.

3.2.3. Spots for beam modelling

The sigma values for the spots modelled by RayStation have a monotonically decreasing dependence with the energy. To compare with data in Tables 1 and 2, RayStation sigma value for 71.2 MeV is 7.83 mm, for 140.8 MeV is 4.19 mm and for 218.7 MeV is 3.04 mm.

An example of Gaussian spots modelled by RayStation compared to the measurements is provided in Fig. 2 for the spot in air at isocenter for 71.2 MeV and 218.7 MeV. Adequate agreement can be observed, although the graph suggests that the fit could be improved by including a second Gaussian with low relative weight and high sigma. This trend was found for all the energy levels in our synchrotron.

3.3. Absolute dose values

The value of k_Q determined for our Advanced Markus chamber was 1.005. Absolute dose values were provided to the TPS to determine the number of protons per monitor unit with respect to the energy. We fitted the number of protons per MU determined by RayStation during beam modelling to beam energy, obtaining the cubic polynomial:

$$NP = 6.093E^3 - 7810E^2 + 5.281 \times 10^6 E + 6.248 \times 10^7 \quad (2)$$

Where NP is the number of protons per MU, and E is the energy of the beam, expressed in MeV. The R^2 of the fit is unity.

Measured dose values vary between 0.7332 cGy/MU for the minimum energy and 0.6603 cGy/MU for the maximum energy. Computed dose values differ with respect to measured values between −0.21% and 0.04%.

The results presented in the paper up to this point refer to the data used for commissioning the system and building the beam model in RayStation. The following sections present results of validation tests performed to check that the model was accurate.

Table 1
Sigma values and their differences for 1D and 2D Gaussian fits with EBT3 and Lynx. Differences in major and minor sigmas between both detectors are also shown. The eccentricity of the spot is calculated as the ratio of the sigmas of the 2D fit.

Energy (MeV)	Quantity	EBT3	Lynx	Diff. (mm)
71.2	σ_M(2D) (mm)	8.10	8.15	0.05
	σ_m(2D) (mm)	7.72	7.92	0.20
	σ_M(1D) (mm)	7.95	7.99	0.04
	σ_m(1D) (mm)	7.64	7.74	0.10
	σ_M(2D)-σ_M(1D) (mm)	0.15	0.16	
	σ_m(2D)-σ_m(1D) (mm)	0.08	0.18	
	Eccentricity	1.049	1.028	
140.8	σ_M(2D) (mm)	4.30	4.40	0.10
	σ_m(2D) (mm)	4.00	4.18	0.17
	σ_M(1D) (mm)	4.13	4.35	0.22
	σ_m(1D) (mm)	3.80	4.10	0.30
	σ_M(2D)-σ_M(1D) (mm)	0.17	0.05	
	σ_m(2D)-σ_m(1D) (mm)	0.20	0.08	
	Eccentricity	1.074	1.052	
218.7	σ_M(2D) (mm)	3.06	3.11	0.05
	σ_m(2D) (mm)	2.79	2.93	0.15
	σ_M(1D) (mm)	2.97	3.06	0.08
	σ_m(1D) (mm)	2.75	2.89	0.14
	σ_M(2D)-σ_M(1D) (mm)	0.09	0.05	
	σ_m(2D)-σ_m(1D) (mm)	0.04	0.04	
	Eccentricity	1.096	1.058	

3.4. Range shifter modelling

The ionization potential calculated for the range shifter was 61.99eV; this was the value used for range shifter modelling. Absolute dose measurements taken with the range shifter in use were within 2.1% of the values calculated by RayStation (the calculated dose was higher than the measured dose). Fig. 3 shows plots of IDDs and spot profiles for the maximum and minimum of the set of 9 energy levels evaluated, confirming that spot modelling using the open beam set of data was good.

3.5. Validation measurements

3.5.1. SOBP fields

These measurements provide a validation of dose calculations, and also of the accuracy of the Monte Carlo correction to the measured IDDs. Table 4 shows the differences in the calculated and measured values of absorbed dose with respect to field size. The measurements displayed were acquired with a Farmer chamber for all fields except those of 2 × 2cm and 3 × 3cm. The values displayed for these fields were acquired with a Semiflex 3D chamber. Values for these fields measured with a PinPoint 3D chamber are not displayed, but they are similar to those obtained with the Semiflex 3D. The table contains values for several widths and depths of the SOBP. The agreement shows the accuracy of the Monte Carlo correction provided by RayStation to the measured IDDs. The scale of differences between calculations and measurements depended on the field size. Differences are always below ± 2% for field sizes between 5 × 5cm and 20 × 20cm. The differences increase slightly for big fields (30 × 30cm) as well as for small fields (3 × 3cm and 2 × 2cm). The agreement improves for shallower depths in larger field sizes (10 × 10cm and larger). For field sizes smaller than 10 × 10cm the agreement in the values is better at deeper depths. Table 5 shows the agreement in the reference dosimetry test according to TRS-398.

Table 5 summarizes the differences between calculated and measured values of the absorbed dose at various depths through the central axis for several field sizes with SOBP curves of various widths. The agreement supports the accuracy of the Monte Carlo correction to the measured IDDs done by RayStation.

3.5.2. Spots in water

Calculated and measured profiles for single spots in water, with the maximum and minimum available beam energy, are shown in Fig. 3 (only the results for two out of eighteen profiles are presented). The closeness of these profiles indicates that the TPS is accurate in its calculation of the interactions of the beam in water.

3.5.3. Validation of point dose calculations in special situations

These validation tests compare measured and calculated point doses when there is oblique incidence or the dose is off-axis or extended-distance. Differences are indicated as a percentage; a positive percentage indicates that calculated doses are higher than measured doses.

Table 2
Comparison of 1D fits to profiles from microDiamond, EBT3 and Lynx detection systems. The average sigma value is also compared to that of a circular 2D fit.

Energy (MeV)	Detector	σ_m 1D (mm)	σ_M 1D (mm)	Average (mm)	Diff. σdetectors (mm)		σcirc. 2D (mm)	Diff. σcirc. 2D ave 1D (mm)
71.2	Diamond	7.66	7.94	7.80	0.09	0.21		
	EBT3	7.74	8.15	7.94			8.16	0.22
	Lynx	7.74	7.99	7.87			8.03	0.17
89.3	EBT3	6.20	6.43	6.32	0.02	0.04	6.44	0.12
	Lynx	6.23	6.47	6.35			6.47	0.12
108.4	EBT3	5.07	5.38	5.23	0.11	0.06	5.37	0.15
	Lynx	5.18	5.45	5.31			5.41	0.10
126.6	EBT3	4.42	4.72	4.57	0.08	0.04	4.64	0.07
	Lynx	4.50	4.76	4.63			4.71	0.08
140.8	Diamond	3.97	4.24	4.10	0.15	0.13		
	EBT3	3.95	4.22	4.09			4.15	0.06
	Lynx	4.10	4.35	4.22			4.29	0.06
160.9	EBT3	3.55	3.80	3.68	0.10	0.09	3.79	0.11
	Lynx	3.66	3.90	3.78			3.84	0.06
178.0	EBT3	3.24	3.48	3.36	0.12	0.12	3.44	0.08
	Lynx	3.37	3.59	3.48			3.53	0.05
194.9	EBT3	2.99	3.25	3.12	0.14	0.10	3.17	0.05
	Lynx	3.14	3.35	3.24			3.29	0.05
218.7	Diamond	2.71	2.97	2.84	0.18	0.09		
	EBT3	2.76	2.97	2.87			2.94	0.07
	Lynx	2.89	3.06	2.97			3.02	0.04

Table 3
Differences in the major and minor sigma values for several gantry angles. Differences are relative to the sigma at 0° gantry position.

Gantry angle	71.2 MeV		140.8 MeV		218.7 MeV	
(deg)	$\Delta\sigma_M$ (mm)	$\Delta\sigma_m$ (mm)	$\Delta\sigma_M$ (mm)	$\Delta\sigma_m$ (mm)	$\Delta\sigma_M$ (mm)	$\Delta\sigma_m$ (mm)
180	0.11	0.16	0.02	−0.04	−0.05	−0.05
210	0.01	0.12	0.02	0.01	−0.02	−0.03
240	−0.05	0.05	−0.16	−0.07	0.04	0.02
270	−0.07	0.02	−0.21	−0.03	0.07	0.10
300	0.02	0.11	−0.11	0.05	−0.06	0.03
330	0.10	0.13	−0.02	0.03	−0.06	−0.02
0	0.00	0.00	0.00	0.00	0.00	0.00
30	0.06	0.06	0.00	0.01	0.07	0.04
60	−0.02	0.14	−0.07	0.03	−0.01	0.01
90	0.01	0.04	−0.12	0.08	−0.04	0.01
120	0.00	0.04	−0.20	0.02	−0.03	0.07
150	0.04	0.10	−0.12	−0.04	0.03	0.04

- Off-axis: Differences in the four fields tested were 1.7%, 1.7%, −0.5%, and 0.6%.
- Oblique incidence: Differences in the three fields tested were (in order of increasing depth) 0.8%, 1.1% and 0.8%.
- Extended-distance: Differences were (in order of increasing distance between source and detector): 2.0% and 1.8%. Maintaining the same source-to-detector distances but with the 3.9 cm range shifter and the detector at a depth of 11 cm in water, the differences were: 2.3% and 2.4%.

3.5.4. Clinical cases

The results of the measurements done with the IBA Matrix detector to check the beam model in clinical cases are displayed in Table 6. The approximate size of the encompassing field is also given. Gamma index checks were calculated for (3%, 3 mm) and (2%, 2 mm). Appended in the table is the information on a similar check of the TRS-398 with a 10 cm × 10 cm field size and a SOBP depth range from 10 to 20 cm.

Table 7 gives the results of the quality assurance test performed with radiochromic film on a set of clinical cases.

4. Discussion

4.1. IDD corrections and uncertainties

The impact of correcting measured IDD by the ratio of the stopping power of water-to-air is small. This ratio is almost independent of proton energy except at very low residual ranges (correction amount is 2% below 1 mm). From the TRS-398 formula for calculating $s_{w,air}$ from the residual range, it can be seen that the correction is more relevant at lower energies, where there is less range straggling and so the Bragg peak is narrower in the proximal to distal direction. Nevertheless, we used the corrected curves for our beam modelling, as recommended in TRS-398. The relevance of this correction is, however, arguably less than that of the clinical practice of using a value of 1.1 for relative biological effectiveness (RBE), which entails an uncertainty in the determination of the biological dose which is largest at most distal part of the proton track (Luhr et al., 2018; Sorensen et al., 2021).

The measurements obtained with an ionization chamber along the central axis of several SOBP fields demonstrate that the RayStation's Monte Carlo correction to IDD measurements is accurate. Note that this test considered that extended field calculations rely on an accurate model of the physical behaviour of the pencil beam (as delivered by the proton system) both with depth over the set of IDD curves and also laterally through the spot.

With respect to the measurement uncertainty of the beam range in water, we assessed the setup geometrical accuracy and the measurement global reproducibility. These data provided an estimation of range measurement uncertainty in water of 0.1 mm, which has negligible clinical impact.

4.2. Spot modeling and sigma uncertainty

A pencil beam's lateral distribution (often referred to as the "spot in air") is elliptical and the ellipse rotates with the gantry angle. The model in RayStation approximates this behaviour by using a single Gaussian model with revolution symmetry (a circular 2D Gaussian) to provide a dose calculation for any situation. The eccentricity of the ellipse is small and increases with increasing energy. With the Hitachi system, it is specified that the ratio of major and minor sigma values should be below 1.1. We found the beam met this condition and demonstrated that the RayStation's model provides a good approximation for the calculation of the dose in clinical plans. Sigma values based on Lynx, microDiamond

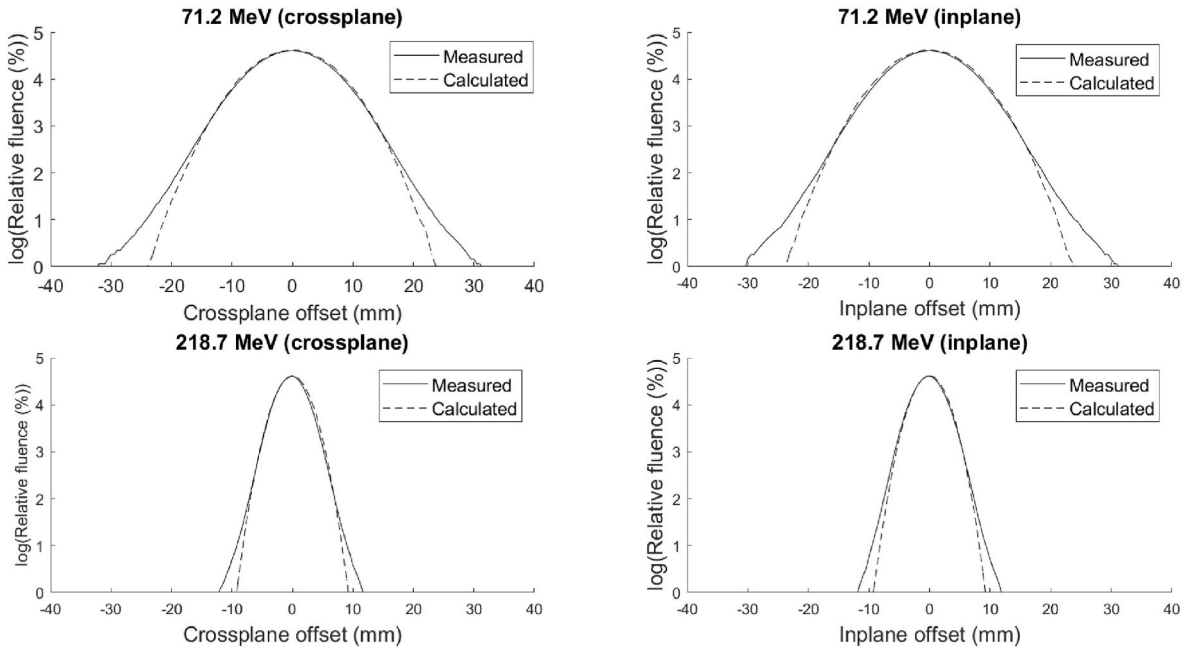

Fig. 2. Comparison between measured and modelled spot profiles. RayStation modelled the spots to a Gaussian distribution.

and EBT3 films measurements were in good agreement and mainly within 0.2 mm, which is also the maximum difference found in the sigma determination through different fits. Comparison of 1D fits through the detector axis with 2D elliptical and circular fits indicated good agreement, with sigma estimations generally within 0.2 mm of each other. These results are congruent with the findings of Grevillot et al., (2018), who concluded that spot sizes could be determined with an uncertainty of less than 0.3 mm. Similar to us, they used radiochromic film, a synthetic PTW 60019 microDiamond detector, and a Lynx scintillator to determine lateral distributions in their proton and light ion beam (Grevillot et al., 2018). The difference in spot size with respect to gantry rotation was also less than 0.21 mm for all gantry angles tested. Determining spot sigma with this accuracy resulted in adequate model performance.

The spot model implemented and used for clinical dose calculations in our TPS is a single Gaussian model. The accuracy of this model for dose calculations has been shown. Using the orthogonal profiles through the detector (gantry) axes is adequate, simplifies data processing and reduces the time required for beam commissioning.

4.3. Small field dose calculations

Spot modelling has an impact on small field dose calculations. The behaviour of the RayStation spot model with small fields is adequate. However, modelling the spot as a double Gaussian, as suggested by the spot profile comparison, would improve dose calculations in these situations. A double Gaussian model would include a second Gaussian with a large sigma and small weight (a few percentage points compared with the primary Gaussian), which would essentially reduce the dose calculated for the centre of the spot and increase the dose close to the penumbra area of the spot. Such increase in the dose is indicated in order to accommodate for the high angle, single scattering events that affect low dose areas of profiles. When carrying out summation of multiple spots in a small field area, the result of using a double Gaussian model would be a smaller dose value for the center of the field compared with what a single Gaussian model would render. Our tests with clinical plans show that, although all plans had sufficiently high gamma index pass rates for (3%, 3 mm), some plans with smaller fields had noticeably worse pass rates for (2%, 2 mm). We would expect single spot modelling with a double Gaussian to improve gamma index results.

Zhu et al., (2013) modelled their Hitachi system for use with Eclipse version 8.120 and 8.917 (Varian Medical Systems, Palo Alto, CA). In their case, using a double Gaussian modelling for the proton beam fluence had a significant impact on dose calculations.

4.4. Range shifter

Range shifter modelling using the open beam data works well. We also checked the beam model's ability to handle oblique incidence, off axis doses, and doses with an air gap; the TPS dealt with these situations properly. The paper of Saini et al. reported the commissioning of RayStation version 4.51; in this version the modelling of the range shifter was not accurate when employed with large air gaps when using the pencil beam algorithm; however, they showed that RayStation Monte Carlo was much more accurate when dealing with these situations. This is in line with our results using Monte Carlo in version 9B.

4.5. Absolute dose values and their uncertainty

The clinical model of our proton beams was that of RayStation version 9B. The results provided in this work correspond to this version. An IROC (Houston, TX) audit for the output calibration at the reference point and also of an end-to-end test using a brain anthropomorphic phantom with known SPR values was successfully performed before starting clinical treatments. Also, we checked the absolute dose values for the reference 10 cm × 10 cm field proposed in TRS-398 by using a different PTW 30013 Farmer chamber that was calibrated independently in terms of $N_{D,w}$; differences in absolute dose values were within 1%.

This difference is mainly attributed to the use of a Monte Carlo calculated k_Q for the dose determination in the user beam. TRS-398 (International Atomic Energy Agency IAEA, 2000) stated this uncertainty to be 1.7% in proton beams, which is the main contribution to the total uncertainty (which also includes the ^{60}Co calibration at a SSDL) in the determination of the absorbed dose with a cylindrical chamber, which is 2.0%. The amount of difference seen with the two sets of Farmer and electrometer is within 1%, so we consider the results of these two tests to be in full agreement within our estimated uncertainty for k_Q. The estimated uncertainty for the measurements done with the Advanced Markus chamber, which was calibrated with ^{60}Co in a SSDL,

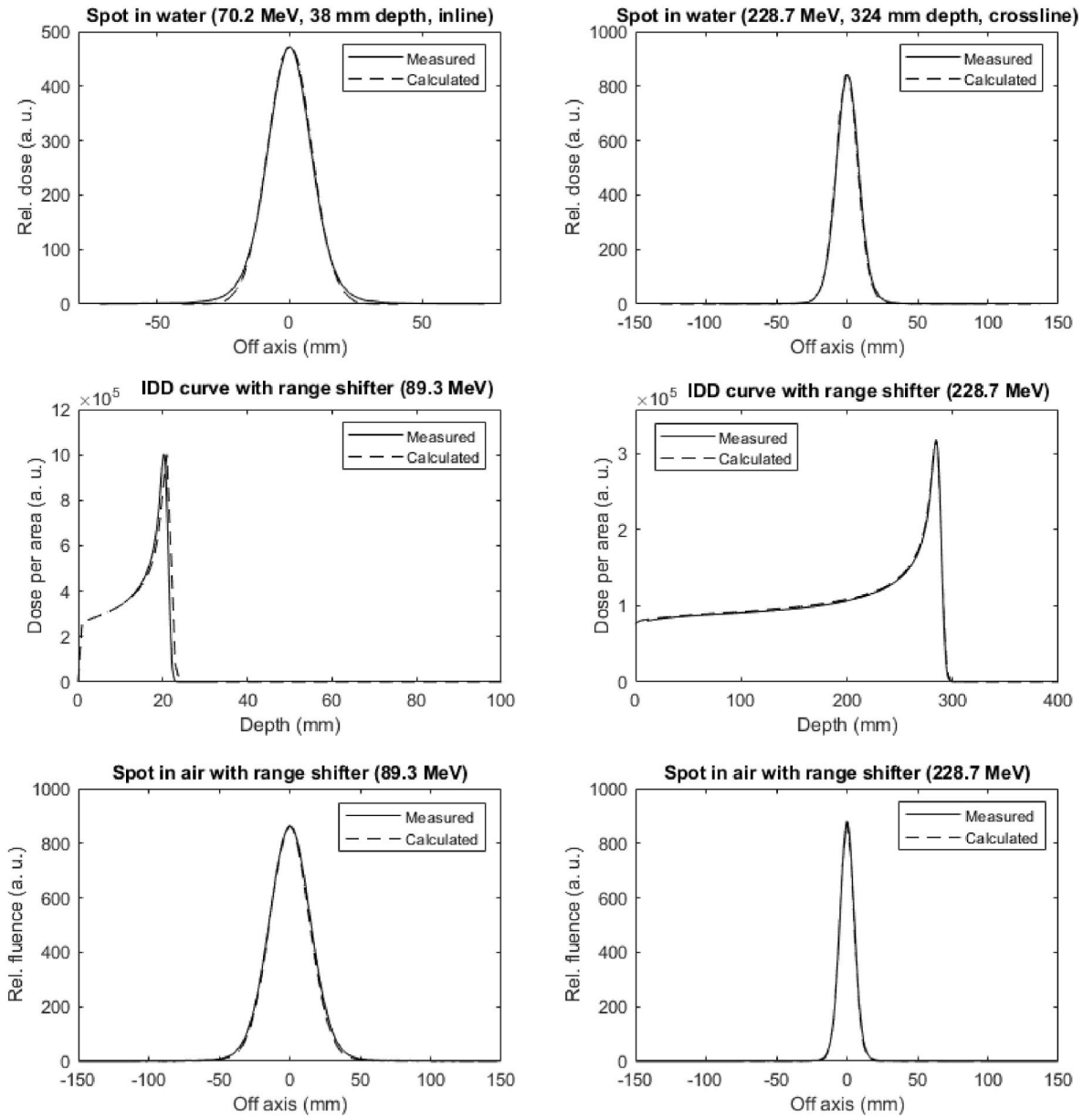

Fig. 3. Upper row: measured and calculated spots in water for 70.2 MeV (inline profile, left) and 228.7 MeV (crossline profile, right). Middle row: measured and calculated IDD curves with range shifter for 89.3 MeV (left) and 228.7 MeV (right). Lower row: measured and calculated spots in air with range shifter for 89.3 MeV (left) and 228.7 MeV (right).

when performing measurements in monoenergetic beams, is 2.3% (International Atomic Energy Agency IAEA, 2000).

The total amount of time needed to perform the clinical commissioning lasted almost four months (12 working hours per day), and also included other tasks such as CT calibration and its validation, work on the clinical dosimetry and workflow training to the personnel. Measurements for beam modelling were acquired during the first five weeks and included detector commissioning and repetition of measurements to ensure their accuracy. Validation measurements were acquired during approximately 5 weeks at the end of the commissioning.

We also checked the dose calculations with version 10A as RaySearch requested of customers using the same beam model. The main difference between versions 9B and 10A is the GPU proton dose calculation performed in the latter. Fracchiolla et al., (2021) compared dose distributions resulting from Monte Carlo dose calculations performed in the CPU with those on the GPU, finding good agreement (within Monte Carlo intrinsic statistical fluctuations). The results of our comparison between dose calculations and measurements with version 10A are similar to those with version 9B, a finding which is in line with the conclusions of Fracchiolla et al., (2021). Our hospital is currently using version 10A.

5. Conclusion

The Monte Carlo beam model for proton beams generated in a synchrotron has been extensively validated. The Monte Carlo correction to the measured IDD curves for beam modelling is accurate. Spot modelling by application of a single circular Gaussian function to the physical pencil beam generated in a synchrotron is adequate and can be used for dose calculations in small fields. A double-Gaussian model for the spot might improve small field dose calculations. Range shifter modelling using open beam data works well. Patient treatment plans can be calculated accurately and safely.

Table 4
Differences between calculated and measured dose values at the center of several SOBP curves for different field sizes, and SOBP depths and widths. Values were measured with a Farmer chamber except for field sizes of 2 × 2cm and 3 × 3cm, which were measured with a Semiflex 3D chamber.

Field size	Prox. range	Distal range	Meas. depth	Calc. dose	Meas. dose	Diff.
(cm^2)	(cm)	(cm)	(cm)	(Gy)	(Gy)	(%)
2 × 2	5	10	7.5	2.002	1.929	3.8
2 × 2	10	20	15.0	2.047	1.988	2.9
2 × 2	15	20	17.5	2.090	2.020	3.5
2 × 2	20	30	25.0	2.056	2.019	1.8
3 × 3	5	10	7.5	2.004	1.946	3.0
3 × 3	10	20	15.0	2.027	1.988	2.0
3 × 3	15	20	17.5	2.071	2.037	1.7
3 × 3	20	30	25.0	2.059	2.028	1.5
5 × 5	5	10	7.5	2.000	1.983	0.9
5 × 5	10	20	15.0	2.011	1.990	1.1
5 × 5	15	20	17.5	2.026	2.019	0.3
5 × 5	20	30	25.0	2.046	2.012	1.7
7 × 7	5	10	7.5	2.012	1.988	1.2
7 × 7	10	20	15.0	2.024	1.995	1.4
7 × 7	15	20	17.5	2.036	2.023	0.6
7 × 7	20	30	25.0	2.020	2.000	1.0
10 × 10	5	10	7.5	1.992	1.995	−0.2
10 × 10	10	20	15.0	2.025	2.001	1.2
10 × 10	15	20	17.5	2.050	2.021	1.5
10 × 10	20	30	25.0	2.042	2.012	1.5
15 × 15	5	10	7.5	1.993	1.994	0.0
15 × 15	10	20	15.0	2.024	2.006	0.9
15 × 15	15	20	17.5	2.049	2.024	1.2
15 × 15	20	30	25.0	2.054	2.020	1.7
20 × 20	5	10	7.5	2.009	1.998	0.6
20 × 20	10	20	15.0	2.034	2.007	1.4
20 × 20	15	20	17.5	2.057	2.028	1.4
20 × 20	20	30	25.0	2.044	2.023	1.0
30 × 30	5	10	7.5	1.999	2.007	−0.4
30 × 30	10	20	15.0	2.087	2.062	1.2
30 × 30	15	20	17.5	2.115	2.072	2.1
30 × 30	20	30	21.0	2.074	2.027	2.3

Table 5
Summary of differences between calculations and measurements, with a Farmer chamber, for single points at various depths along the central axis (PDD), for several field sizes with SOBP curves of various widths.

Field (cm^2)	SOBP (cm)	Mean diff. (%)	Min. diff. (%)	Max. diff. (%)
5 × 5	5–10	0.8	0.4	1.2
5 × 5	10–20	0.5	−0.1	1.2
5 × 5	15–20	1.2	0.3	1.7
10 × 10	5–10	0.3	0.0	0.8
10 × 10	10–20	0.6	0.2	1.3
10 × 10	15–20	0.6	−0.6	1.4
20 × 20	5–10	0.2	−0.1	0.8
20 × 20	10–20	0.7	0.1	1.8
20 × 20	15–20	0.9	0.0	1.6

Table 6
Measurements relating to clinical cases checked using an IBA Matrix 2D ionization chamber array. The percentage of points passing the local gamma index criterion is displayed. Depth is expressed in cm; the medium used was acrylic.

Case	Plane depth (cm)	Encompassing field size (cm^2)	Gamma index (3%, 3 mm)	Gamma index (2%, 2 mm)
Head and neck #1	1	15 × 15	100.0	94.9
	2		99.7	95.5
	3		99.9	98.5
	4		98.7	91.0
	5		100	96.4
	12		99.3	95.2
Cavum #1	3	6.5 × 6.5	98.7	78.9
	5		92.7	79.7
	7		93.1	82.8
Cavum #2	3	6 × 6	100	87
	5		95.9	81.1
	7		94.9	81.4
Cranial #1	3	4 × 4	97.6	92.7
	5		100.0	90.7
	7		95.2	88.1
Cranial #2	3	4 × 4	96.9	92.2
	5		95.1	82.0
	7		89.8	78.0
Head and neck #2	3	7.5 × 7.5	100.0	99.3
	5		98.5	92.5
	7		94.6	90.7
TRS-398 10 × 10 cm^2 field, SOBP between 10 and 20 cm	10	10 × 10	100.0	100.0
	11		100.0	100.0
	12		100.0	100.0
	13		100.0	100.0
	14		100.0	100.0
	15		100.0	100.0

Table 7
Gamma passing rate for clinical cases as determined by means of radiochromic film. The film was placed in acrylic at the depths indicated.

Localization	Plane depth (cm)	Gamma passing rate (3%, 3 mm)
Cranial #1	4	91.3
	6	87.1
Cranial #2	4	95.8
	6	98.8
Head and neck #1	3	99.4
	5	98.9
TRS-398	4	97.4
	13	95.6

Author statement

Juan-Diego Azcona: Conceptualization, data curation, formal analysis, investigation, methodology, supervision, validation, project administration, writing – original draft. **Borja Aguilar:** Data curation, methodology, investigation, software, formal analysis, resources, visualization, writing – review and editing. **Álvaro Perales:** Data curation, formal analysis, methodology. **Ramón Polo:** Data curation, formal analysis, validation. **Daniel Zucca:** Data curation, formal analysis, validation. **Leticia Irazola:** Data curation, writing – review and editing. **Alberto Viñals:** Validation. **Pablo Cabello:** Validation. **José-Miguel Delgado:** Resources. **Diego Pedrero:** Validation, resources. **Rocío Bermúdez:** Validation. **Roser Fayos-Solá:** Validation. **Carlos Huesa-Berral:** Software. **Javier Burguete:** Formal analysis, methodology, software, writing – review and editing.

Declaration of competing interest

The authors declare that they have no known competing financial interests or personal relationships that could have appeared to influence the work reported in this paper.

Data availability

Data will be made available on request.

Acknowledgements

Michael Herman, Ph. D., Nicholas Remmes, Ph. D., Daniel Mundy, Ph. D., Jon Kruse, Ph. D., Amanda Deisher, Ph. D., Chris Beltran, Ph. D. and Keith Furutani, Ph. D. (Mayo Clinic, MN), and Jose Alonso, Ph. D. (Lawrence Berkeley Laboratory, CA) are gratefully acknowledged for helpful scientific discussions.

References

Arjomandy, B., et al., 2019. AAPM task group 224: comprehensive proton therapy machine quality assurance. Med. Phys. 46, e678–e705.

Dong, L., 2015. Clinical commissioning of proton beam. In: Das, I.J., Paganetti, H. (Eds.), Principles and Practice of Proton Beam Therapy, American Association of Physicists in Medicine AAPM (Monograph 37). Medical Physics Publishing, Madison, Wisconsin.

Farr, J.B., et al., 2021. Clinical commissioning of intensity-modulated proton therapy systems: report of AAPM Task Group 185. Med. Phys. 48, e1–e30.

Farr, J.B., et al., 2018. Development, commissioning, and evaluation of a new intensity modulated minibeam proton therapy system. Med. Phys. 45, 4227–4237.

Fracchiolla, F., et al., 2021. Clinical validation of a GPU-based Monte Carlo dose engine of a commercial treatment planning system for pencil beam scanning proton therapy. Phys. Med. 88, 226–234.

Gillin, M.T., et al., 2010. Commissioning of the discrete spot scanning proton beam delivery system at the University of Texas M.D. Anderson Cancer Center, Proton Therarapy Center. Houston. Med. Phys. 37, 154–163.

Gottschalk, B., 2018. Physics of proton interactions in matter. In: Paganetti, H. (Ed.), Proton Therapy Physics, second ed. CRC Press. Taylor and Francis Group, Boca Raton, FL.

Grevillot, L., et al., 2018. Implementation of dosimetry equipment and phantoms at the MedAustron light ion beam therapy facility. Med. Phys. 45, 352–369.

International Atomic Energy Agency IAEA, 2000. Absorbed Dose Determination in External Beam Radiotherapy: an International Code of Practice for Dosimetry Based on Standard of Absorbed Dose to Water. IAEA Technical Report Series 398) (Vienna).

ICRU International Commission on Radiation Units and Measurements, 1984. Radiation Dosimetry: Electron Beams with Energies between 1 and 50 *MeV ICRU Report No. 35*. International Commission on Radiation Units and Measurements, Bethesda, MD.

Kuess, P., et al., 2017. Lateral response heterogeneity of Bragg peak ionization chambers for narrow-beam photon and proton dosimetry. Phys. Med. Biol. 62, 9189–9206.

Lin, L., et al., 2013. A novel technique for measuring the low-dose envelope of pencil-beam scanning spot profiles. Phys. Med. Biol. 58, N171–N180.

Luhr, A., et al., 2018. Radiobiology of proton therapy": results of an international expert workshop. Radiother. Oncol. 128, 56–67.

Moyers, M.F., et al., 2020. Physical Uncertainties in the Planning and Delivery of Light Ion Beam Treatments (Report of the AAPM Task Group 2020). American Association of Physicists in Medicine AAPM, Alexandria, VA.

Newhauser, W.D., Zhang, R., 2015. The physics of proton therapy. Phys. Med. Biol. 60, R155–R209.

Paganetti, H., 2012. Range uncertainties in proton therapy and the role of Monte Carlo simulations. Phys. Med. Biol. 57 (11), R99–R117.

Palmans, H., 2018. Absolute and reference dosimetry. In: Paganetti, H. (Ed.), Proton Therapy Physics, second ed. CRC Press. Taylor and Francis Group, Boca Raton, FL.

Russo, S., et al., 2017. Characterization of a commercial scintillation detector for 2-D dosimetry in scanned proton and carbon ion beams. Phys. Med. 34, 48–54.

Saini, J., et al., 2016. Clinical commissioning of a pencil beam scanning treatment planning system for proton therapy. Int. J. Particle Ther. 3 (1), 51–60.

Saini, J., et al., 2017. Dosimetric evaluation of a commercial proton spot scanning Monte-Carlo dose algorithm: comparisons against measurements and simulations. Phys. Med. Biol. 62, 7659–7681.

Sorensen, B.S., et al., 2021. Does the uncertainty in relative biological effectiveness affect patient treatment in proton therapy? Radiother. Oncol. 163, 177–184.

Taylor, P.A., et al., 2017. Pencil beam algorithms are unsuitable for proton dose calculations in lung. Int. J. Radiat. Oncol. Biol. Phys. 99 (3), 750–756.

Zhu, X.R., et al., 2013. Commissioning dose computation models for spot scanning proton beams in water for a commercially available treatment planning system. Med. Phys. 40, 041723, 1:15.